Manifestation of coherent effects in the conductivity of superconductor/insulator/normal-metal/insulator/superconductor junctions

I. P. Nevirkovets,* S. E. Shafranjuk,† and J. B. Ketterson‡
Department of Physics and Astronomy, Northwestern University, Evanston, Illinois 60208, USA
(Received 30 December 2002; revised manuscript received 11 April 2003; published 25 July 2003)

An experimental and theoretical study is presented of coherent effects in electron transport in the double-barrier SINIS junctions (where S, I, and N denote a superconductor, insulator, and normal metal, respectively). The appearance of a steplike subgap structure in the current-voltage characteristics of the $Nb/Al/AlO_x/Al/AlO_x/Al/Nb$ superconducting junctions at a voltage $V \sim \Delta_{Nb}/e$ (where Δ_{Nb} is the superconducting energy gap of Nb) is interpreted as a manifestation of a nonequilibrium supercurrent at *finite dc bias voltage* (Finite-Bias Josephson Effect). The origin of this effect lies in the energy-band structure associated with a set of macroscopic quantum states characteristic of a SINIS junction. Specifically, the junction can have an energy level near energy Δ_{Nb}, which provides an additional channel for dc Josephson current at $V \sim \Delta_{Nb}/e$. In addition, sharp features in the conductivity at a voltage near the gap-sum voltage were observed in both SINIS and SINININIS junctions, implying correlated quasiparticle tunneling in multiple-barrier junctions. Our theoretical model provides a good qualitative description of the quasiparticle conductivity, including narrow peaks at finite voltage and a zero-voltage anomaly observed on some samples, and suggests an alternative explanation of a feature interpreted earlier as gap-difference feature associated with the tunneling extraction of quasiparticles from the middle Al layer.

DOI: 10.1103/PhysRevB.68.024514 PACS number(s): 74.50.+r, 74.78.Fk, 73.40.Gk

I. INTRODUCTION

In recent years, systems based on an SNS structure (where S is a superconductor and N is a normal metal), in which the phase-coherence is preserved (in at least one dimension) over a distance comparable to the BCS coherence length, ξ_{BCS}, have been extensively studied.[1–3] In such a system, the phase-coherent transport occurs as a consequence of phase-correlated Andreeev reflections (AR) at both the SN and NS interfaces, but is strongly dependent on the device geometry and its interaction with the environment. If the size of the N layer is also comparable to ξ_{BCS}, the AR and the electron-hole interference inside the potential well (formed by the minimum of the pairing potential between the S electrodes) leads to localized Andreev bound-state (ABS) levels[4,5] with quantized energies E_n, which may carry a supercurrent. Experimental and theoretical work on phase-coherent transport in SNS systems[1] includes studies of the energy dependence of the Andreev reflection processes,[6] and proposals to probe the ABS levels directly.[7,8] However, to our knowledge, no clear experimental evidences of a connection between the supercurrent and the ABS has been obtained up to now.

Introducing insulating barriers I at the interfaces between S and N substantially changes the properties of the system. For most of the SINIS junctions studied, the transparency of the insulating barriers is less than unity, by several orders of magnitude. In this case, the contribution to the conductivity involving AR is usually regarded as small; it is assumed that the AR at the two interfaces are uncorrelated, so that in order to transfer a Cooper pair (CP) through the composite INI barrier, the probabilities of the two sequential AR are multiplied, yielding a very low resultant probability. However, it was argued by the present authors that this probability may be greatly enhanced if the AR at the two interfaces are coherent.[9] The physical idea is based on the fact that the Andreev reflection occurs on a relatively long-distance scale $\xi_{BCS} \gg p_F^{-1}$ (p_F being the Fermi momentum). Then, if thickness d_N of the middle N layer is comparable to ξ_{BCS}, the electron-hole interference may form a standing wave with a wave vector $q_s \simeq p_e - p_h \sim 1/\xi_{BCS} \ll p_F$. For $d_N \sim 1/q_s$, the standing wave corresponds to a resonant ABS energy level E_A (in general, there is a set of standing waves with energies E_n). Transmission via resonant levels is expected to be much more efficient than transitions via the continuum states. For this reason, the critical Josephson current may be enhanced in systems with sharp ABS. Experimental evidence of such coherent effects in $Nb/Al/AlO_x/Al/AlO_x/Al/Nb$ junctions was recently reported.[10–13] Specifically, an anomalous Josephson critical current $I_c^{(0)}$ (Ref. 10), a subgap structure,[11] and an unusual behavior under high-frequency irradiation[12,14,15] have been observed. Coherent effects in the SINIS junctions were also considered theoretically.[9,10,16,17] In spite of this work, the excitation spectrum and phase-coherent transport in such junctions deserves further study. Furthermore, SINIS junctions represent a rich physical system, and are potentially useful for many applications.

An interesting steplike structure was observed recently in the vicinity of voltage Δ_{Nb}/e (here Δ_{Nb} is the energy gap of Nb) in the current-voltage characteristics (CVC) of $Nb/Al/AlO_x/Al/AlO_x/Al/Nb$ junctions.[10,11] A similar feature, and in the same voltage region, was later reported by Bartolome *et al.*[18] It was suggested that the feature is related to phase-coherent transport; specifically, it may be the first direct observation of a resonant dc supercurrent carried by an ABS.[11] An important test of the ABS origin of this feature is provided by its response to a magnetic field H. In a recent work, we reported on a measurement of the magnetic-field dependence of the height of the step, $I_c^{(1)}$, with improved

resolution,[13] so that comparison with the theory could be made more reliably. In the present work, we report a detailed theoretical interpretation of the effect. The theory has also been extended to treat the system self-consistently. A numerical calculation of the $I_c^{(1)}(H)$ dependence is carried out based on the theory, and a comparison with the experimental data is made.

The proposed theoretical interpretation is also capable of describing other features we have observed in Nb/Al based junctions with the SINIS and SINININIS structure: a zero-bias anomaly and sharp peaks in the vicinity of voltage $2\Delta_{Nb}/e$. A zero-bias anomaly has been observed on a number of mesoscopic systems,[19–22] including sandwich-type superconductor-semiconductor-superconductor junctions with the SINIS structure,[23] and is commonly regarded as evidence for phase-coherent transport.

According to our observations, a narrow peak (sometimes a few peaks) in the conductivity at a voltage $2\Delta/e$ is a characteristic property of SINIS-type structures. To our knowledge, there is no satisfactory explanation as to why the width of such a peak (or peaks) can be considerably less than the width of the BCS singularity $\propto E/\sqrt{E^2-\Delta^2}$ (where E is the quasiparticle energy and Δ is the superconducting energy gap); this fact is naturally explained by our theory as a manifestation of coherent effects in the quasiparticle transport. In addition, it follows from our theoretical model that a feature in the CVC regarded earlier as a manifestation of an extreme gap enhancement in Al due to tunnel extraction of quasiparticles,[24] can more naturally be explained as a result of ''doubling'' of an energy level situated near Δ.

This paper is organized as follows. In Sec. II we present experimental results on the transport properties of our junctions. In Sec. III we formulate a theoretical model to explain the phenomena observed. The calculations suggest that in a SINIS junction with a very thin N layer (of order a coherence length ξ_{BCS}, in S) and moderate barrier transparency α, the ABS structure consists of a set of narrow and well resolved energy levels. The level at $V \simeq \Delta_{Nb}/e$ is responsible for a supercurrent channel, a phenomenon which we call the Finite-Bias Josephson Effect (FBJE). In Sec. IV, we discuss our experimental data and theoretical results in more detail. Our conclusions are given in Sec. V.

II. EXPERIMENTAL RESULTS

A. Novel subgap step

The experiments were carried out on SINIS junctions where S and N are Nb and Al, respectively. Details on the fabrication of the structures can be found elsewhere.[10] The junctions were characterized by measuring the CVC between the Nb electrodes.

Figure 1(a) shows the CVC at 1.9 K of a $Nb/Al/AlO_x/Al/AlO_x/Al/Nb$ junction with a thickness $d_{Al}=7$ nm, measured at different values of the magnetic field H applied parallel to the structure layers (curves 1–5 are for 0, 6, 40, 54, and 100 G, respectively; curves 1–4 are displaced from curve 5 and from each other along the current axis by 2 mA for clarity). The CVC display a steplike feature in the

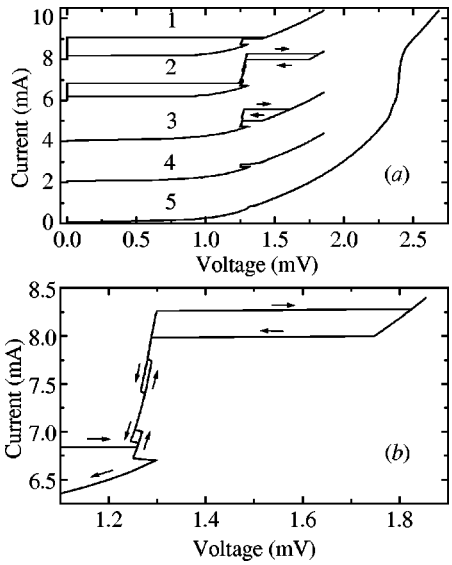

FIG. 1. (a) Typical current-voltage characteristic (CVC) of a $Nb/Al/AlO_x/Al/AlO_x/Al/Nb$ junction at 1.9 K at $H=0$, 6 G, 40 G, 54 G, and 100 G (curves 1–5, respectively). Upper curves are shifted from each other along the current axis by 2 mA for clarity. (b) Magnified portion of the CVC measured at 6 G on showing that the step has multiple branches.

neighborhood of $V=\Delta_{Nb}/e$, which appears as the temperature is lowered below ~ 3 K. The step is sensitive to a weak magnetic field; it disappears above $H \sim 100$ G [curve 5 in Fig. 1(a)], suggesting it is related to coherent transport. The step may have a fine structure, as can be seen from Fig. 1(b). Here, a portion of the CVC [see curve 2 in Fig. 1(a)] is shown on a magnified scale for clarity. Obviously, the step has multiple branches with hysteretic switching between them as the current is changed. The direction of the current development is shown by arrows.

Some other properties of the step are as follows: (1) the position of the step moves towards lower voltages as the temperature is decreased; (2) there is a portion with negative differential resistance at the foot; (3) the height of the step, $I_c^{(1)}$ (measured from the background quasiparticle current to the top) is modulated by H; and (4) the period of the modulation, δH, appears to be closely correlated with that for the zero-voltage supercurrent $I_c^{(0)}$ [see Fig. 2(a)]. These properties distinguish the step from the ordinary ''gap steps'' that appear in the CVC of SIS′IS stacks due to inductive coupling between the junctions[25–27] (in our case, one might assume that the superconducting energy gap is induced in the middle N layer, so that a SINIS junction might be regarded as SIS′ and S′IS junctions connected in series). An additional and remarkable difference between the SINIS junctions and the stacks just mentioned[25–27] is that even if the transparency of the two barriers differs by a factor of two or so, all the significant features in the CVC are closely confined to voltages Δ_{Nb}/e and $2\Delta_{Nb}/e$.

We now turn to the observed diffraction patterns, presented in Fig. 2(a).[28] It is important that the main periodicity of the $I_c^{(1)}(H)$ dependence (solid circles) coincides closely with the periodicity of the $I_c^{(0)}(H)$ dependence (open circles).

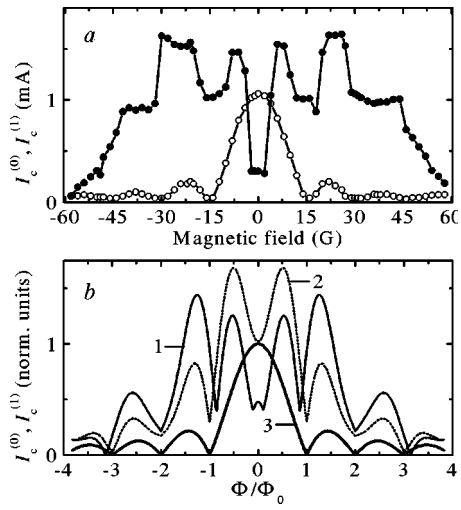

FIG. 2. (a) Fraunhofer patterns $I_c^{(0)}(H)$ (open circles) and $I_c^{(1)}(H)$ (solid circles) of the same Nb/Al/AlO_x/Al/AlO_x/Al/Nb device as Fig. 1, measured at 1.9 K. Lines are guides for the eye. (b) Shown also are the theoretical dependences $I_c^{(1)}(H)$ (curves 1,2) and $I_c^{(0)}(H)$ (curve 3). Curve 2 does not take into account a term proportional to $\sin(\varphi/2+\varphi_3)$, whereas curve 1 does.

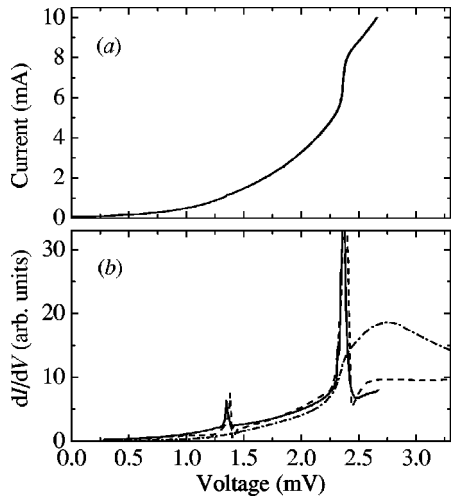

FIG. 3. (a) Current-voltage characteristic (CVC) of the same junction (cf. Fig. 1) at 3 K ($H=0$). (b) Differential conductivity corresponding to the above CVC, which displays the sharp feature at $V\simeq\Delta_{Nb}/e$, a precursor of the novel supercurrent step, and a sharp and narrow peak at $V\simeq 2\Delta_{Nb}/e$ (solid curve). Theoretical differential conductivities for the SINIS and an equivalent SIS junction are shown by the dashed curve and the dash-dotted curve, respectively.

This confirms that the phases of the superconducting (SC) wave functions in the external S electrodes are strongly correlated while the junction is biased at the step. The situation would be different if inductive coupling were the only mechanism of interaction between the junctions, e.g., in the SIS′ IS stack[26]; in that case, if one of the junctions switched to the resistive state, period δH of the second junction (still being in the SC state) would be considerably longer, if S′ is much thinner than the London penetration depth[25] (the case relevant here).

Finally, we consider the temperature dependence of the step. Although the step becomes clearly noticeable in the CVC at a temperature slightly above 2 K, its trace can be found at higher temperatures in the differential conductance. Fig. 3(a) shows typical CVC of a sample described above (cf. Fig. 1) at 3.0 K in the absence of an applied magnetic field; at first sight, it seems to be smooth, but its derivative [see Fig. 3(b), solid curve] displays a sharp feature near a voltage $V=\Delta_{Nb}/e$. At this temperature, the energy gap of the Nb films used in our experiments should be 1.34 mV (as estimated from the Nb-based SIS junctions). Taking this value, one can infer from the experimental curve [solid curve in Fig. 3(b)] that the first sharp feature is situated at a slightly higher voltage of 1.35 mV, whereas the second sharp feature is situated at 2.37 mV, which is lower than expected $2\Delta_{Nb}/e$. The physical basis of such a behavior is suggested in the discussion presented below. Here we note that the feature near $V=\Delta_{Nb}/e$ [cf. Fig. 3(b)] is observed far above the critical temperature of the Al middle layer, which is estimated to be $T_c^{Al}\simeq 1.7$ K for the samples under consideration.

Step height $I_c^{(1)}$ was measured in detail as a function of temperature for the samples described in Ref. 11. In Fig. 4, the dependence is shown for two identical samples (solid and open circles). There is a ''tail'' at higher temperatures and a sharp rise in the vicinity of ~ 2 K, which is reminiscent of the temperature dependence of the zero-voltage Josephson current (see, e.g., Refs. 10,29). This observation suggests that the increase of the step height may be associated with superconducting correlations in the Al layer starting below ~ 2 K. Our theoretical calculations (discussed below) support such an interpretation (solid curve in Fig. 4). As in the former case (cf. Fig. 3), the anomalous current step persists even at temperatures significantly higher than the estimated critical temperature T_c^{Al} of superconducting Al (which should not exceed 2 K for the rather ''dirty'' Al used in these particular samples.[11,30]) Therefore, the origin of the step is not immediately related to intrinsic superconductivity of the middle Al layer.

B. "Quasiparticle" conductivity: sharp features near $2\Delta/e$ and zero-bias anomaly

In order to measure the conductivity of SINIS junctions over a wide range of voltages, we have fabricated some junc-

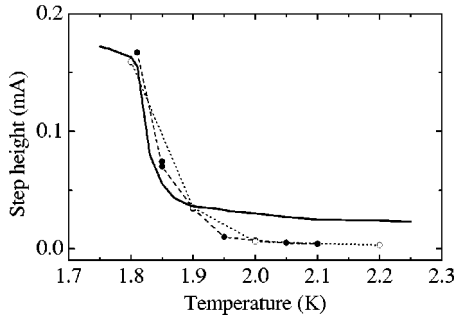

FIG. 4. Temperature dependence of the height of the magnetic-field-sensitive step, $I_c^{(1)}(H)$. Solid and open circles are for two identical samples. The solid curve shows the theoretical dependence calculated for $T_c^{Al}=1.9$ K, $Z=0.3$, and $d_N=\xi_{BCS}$.

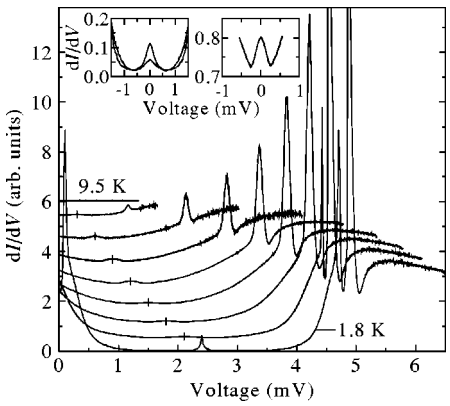

FIG. 5. Conductivity of a Nb/Al/AlO_x/Al/AlO_x/Al/Nb junction at various temperatures. Curves from top to bottom are for: 9.5 K, 8.5 K, 7.5 K, 6.5 K, 5.5 K, 4.5 K, 3.5 K, 2.5 K, and 1.8 K. Left inset: zero-bias feature (shown on a magnified scale) related with the onset of the Josephson current at 1.8 K. Upper curve is for $H=0$; lower curve is for $H=200$ G. Right inset: zero-bias feature which is not related with the Josephson effect (shown on a magnified scale for the 5.5 K curve). For clarity, curves in the main figure are displaced from each other by 0.5 units upward along the dI/dV axis and by 0.3 mV from left to right (starting from the 9.5 K curve) along the voltage axis.

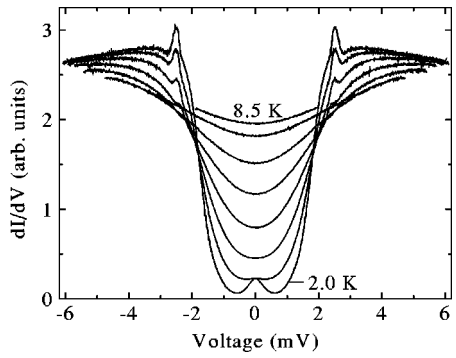

FIG. 6. Conductivity of a Nb/Al/AlO_x/Al/AlO_x/Al/AlO_x/Al/AlO_x/Al/Nb junction at various temperatures. Curves from top to bottom are for: 8.5 K, 8.0 K, 7.0 K, 6.0 K, 5.0 K, 4.0 K, 3.0 K, and 2.0 K.

tions with lower transparency of the barriers as compared with the junctions described above. This weakens the coherent effects (so that, e.g., a step structure near Δ_{Nb}/e does not appear in the CVC, at least in the temperature range used in the experiment), but allows us to reduce undesirable heating effects, and thereby, to measure the CVC up to voltages considerably larger than the gap-sum voltage. Figure 5 shows the differential conductivity of a Nb/Al/AlO_x/Al/AlO_x/Al/Nb junction with a thickness $d_{Al}=6$ nm at different temperatures in the range from 9.5 K to 1.8 K (curves from top to bottom, respectively).

The most pronounced feature of the $dI(V)/dV$ dependence is a narrow peak near a voltage $2\Delta_{Nb}/e$, which appears on a broad maximum also present near the same voltage. These two maxima are characteristic of the SINIS junctions we measured. As can be inferred from Fig. 5, the width of the narrow peak is significantly less than the width of a BCS gap-sum singularity as it appears in ordinary SIS tunnel junctions (where its width, in the absence of spatial variations and anisotropy of the energy gap, is determined by temperature smearing). This experimental fact suggests that coherent effects may play a role in the quasiparticle conductivity, producing sharp features.

In some cases (like that shown in Fig. 5), the peak splits in two at sufficiently low temperatures, so that an additional sharp maximum appears at $V<2\Delta_{Nb}/e$, which was earlier explained as the result of a nonequilibrium stimulation of superconductivity in the middle Al film.[24,31] The "gap-difference" feature in the CVC of SINIS junctions was also discussed by one of us,[32] where an alternative interpretation of its appearance was suggested.

Moreover, a similar narrow peak was also observed in Nb/Al/AlO_x/Al/AlO_x/Al/AlO_x/Al/AlO_x/Al/Nb junctions with the SINININIS structure, which have been fabricated using nominally the same oxidation dosage for barrier formation as the SINIS junctions. The conductivity of the four-barrier junctions at various temperatures is shown in Fig. 6. The zero-bias feature related with Josephson tunneling appears at 2 K (see the bottom curve in Fig. 6), and a peak at $V\simeq 2\Delta_{Nb}/e$ is present, but weaker than that in the double-barrier junctions. The overall shape of the conductivity, with a broad maximum and a peak at $V\simeq 2\Delta_{Nb}/e$, is very similar to the conductivity of the double-barrier junctions. It should be noted that in the case of a SINIS junction, the fact that the position of a steep portion of the CVC roughly corresponds to $2\Delta/e$, may be naively explained as the result of in-series connected SIN and NIS junctions (where the resistance of the N film can be neglected). Such an oversimplified interpretation fails in case of a SINININIS junction, because, if all the junctions were connected in series, two additional (as compared to the SINIS structure) tunnel barriers would contribute significantly to the resistance of the system, so that the gap-related features in the total CVC would be shifted to a considerably higher voltage than $2\Delta/e$. However, this is not the case in the experiment on our Nb/Al-based junctions: obviously, a narrow peak associated with $2\Delta_{Nb}/e$ is positioned at roughly the same voltage for both the two-barrier and four-barrier junctions. We suggest that this behavior is due to a weak, but still present, correlated quasiparticle tunneling between the S electrodes in a multiple-barrier SINININIS junction. Indeed, such a correlated tunneling is expected to be much stronger in the SINIS junctions.

The temperature dependence of the voltage at which the main sharp peak appears, V_p, is shown in Fig. 7; it follows the temperature dependence of the BCS energy gap (shown in Fig. 7 as a solid line) reasonably well, indicating that the peak is indeed a gap-related feature. For better comparison, both dependences are given in normalized units: V_p is normalized to its value at 2 K, whereas the energy gap is normalized to its value at 0 K.

At higher temperatures, the $dI(V)/dV$ dependence of SINIS junctions displays a maximum at zero voltage, which becomes less pronounced at lower temperatures. This zero-bias peak is shown on magnified scale for the 5.5 K curve in the right-hand inset of Fig. 5. The feature is theoretically interpreted below as a consequence of elastic electron-

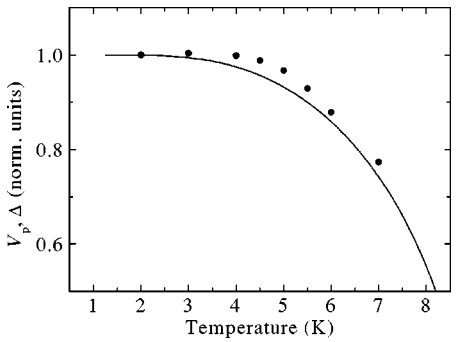

FIG. 7. Experimental temperature dependence of the voltage corresponding to a narrow peak at $V \simeq 2\Delta_{\mathrm{Nb}}/e$ (dots) (cf. Fig. 6). Solid curve corresponds to the BCS temperature dependence of the Nb energy gap (normalized by a maximum value at 0 K) for $T_c^{\mathrm{Nb}} = 9.0$ K. Experimental data are normalized by the peak voltage at 2.0 K.

impurity scattering which can modify the electron density of states at zero energy. Such a zero-bias anomaly is weakly dependent on the magnetic field. This behavior distinguishes it from the zero-voltage feature associated with the ordinary Josephson effect, which is not present in the same temperature range, and appears as a sharp peak only at 1.8 K (the lowest temperature available in the experiment). The latter feature is shown on a magnified scale in the left-hand inset of Fig. 5. The upper curve is for zero magnetic field, and the lower curve is measured in a magnetic field of 200 G applied parallel to the junction plane; one can see that the feature is significantly suppressed by the field.

III. THEORETICAL MODEL

In this section, we develop a theoretical model for SINIS junctions, which describes the basic coherent phenomena observed in the experiment. Although the actual junction geometry is, in reality, SNININS rather than SINIS (due to the Al layers used to form the AlO_x barriers), we will use the latter geometry to simplify the theoretical model. Such an approximation is based on the following reasoning. The net supercurrent through the junction depends on the anomalous Green function $f(x)$ integrated over ζ_p (where x is the coordinate perpendicular to the junction plane, and ζ_p is the electron kinetic energy). For relatively low-transparency barriers (i.e., for $\alpha \ll 1$, where α is the barrier transparency), the supercurrent is expressed via product $f_1 f_2^{\dagger}$, where functions f_1 and $f_2^{\dagger}$ are calculated in the vicinity of the interface but on opposite sides of it; the spatial behavior of $f(x)$ is then quite sensitive to the magnitude of α. For high-transparency SN and NS interfaces (formed by external Nb electrodes and thin adjacent Al layers) we assume $\alpha \leqslant 1$; the pair amplitude is then almost continuous at the interface, and such a SN (NS) sandwich can be regarded as a purely S electrode. On the other hand, at the SIN and NIS interfaces, where $\alpha \ll 1$, the value of $f(x)$ drops significantly. When a bias voltage is applied across the whole device, it drops almost entirely at the SIN and NIS interfaces (but not at the outermost SN and NS interfaces). Therefore, in our case, a simpler SINIS geometry can well represent the actual SNININS structure.

Our approach is based on the quasiclassical, nonstationary, real-time Eilenberger[33] equations (EE):

$$-i\left(\eta v_{\mathrm{F}}\frac{\partial}{\partial x}+\frac{\partial}{\partial t}\right)g=\tilde{\Delta}(x,t)\,\mathrm{Im}\,f+T^R(E,t) \qquad (1)$$

and

$$-i\left(\eta v_{\mathrm{F}}\frac{\partial}{\partial x}+2eiA_z+\frac{\partial}{\partial t}\right)f = 2\tilde{\Delta}(x,t)g-2\tilde{E}(x,t)f+P^R(E,t) \qquad (2)$$

completed by a similar equation for $f^{\dagger}$. In Eqs. (1) and (2), $g(E,x,\eta,t)$ and $f(E,x,\eta,t)$ are normal and anomalous retarded Green functions, respectively, integrated over the kinetic electron energy ζ_p. Here, $\eta=\cos\theta$ (where θ is the angle between the electron momentum $\mathbf{p}$ and the $\hat{\mathbf{x}}$-axis), A_z is the vector potential (associated with an in-plane magnetic field), $\tilde{E}=E+i\langle g\rangle/2\tau_{\mathrm{i}}$, $\tilde{\Delta}=\Delta+i\langle f\rangle/2\tau_{\mathrm{i}}$ (where $\langle\cdots\rangle$ means the averaging over angles of the electron momentum $\mathbf{p}$ and τ_{i} is the elastic scattering time),

$$\Delta(t)=\frac{\lambda(x)}{2}\int dE\,\mathrm{Re}[f(E,x,t)][1-2n_E(t)], \qquad (3)$$

$\lambda(x)$ is the coupling constant, $n_E(t)$ is the nonequilibrium electron distribution function (which generally may also depend on time t), and $g^2-f^2=1$. $T^R(E,t)$ and $P^R(E,t)$ account for the inelastic interaction of electrons with phonons. Such terms originate from the electron-phonon interaction introduced into Eqs. (1) and (2) by using the electron-phonon retarded self energy[34] $\Sigma^R(\mathbf{p},E,t)$. In this way, one may write, e.g., the electron-phonon interaction term $P^R_{\text{e-}ph}$ as

$$P^R_{\text{e-}ph}(E,E-\omega)=\int dt e^{i\omega t}P^R_{\text{e-}ph}(E,t)=\frac{1}{8}N(0)\kappa^2(x)\int d\Omega_{p'}\int d\omega_1(\{D^K_{p-p'}(\omega_1)[g(\omega-E+\omega_1)f(\omega-E)-f(\omega-E+\omega_1)$$
$$\times g(\omega-E)]+D^A_{p-p'}(\omega_1)[g^K(\omega-E+\omega_1)f(\omega-E)-f^K(\omega-E+\omega_1)g(\omega-E)]\}\delta(\omega)-\{D^K_{p-p'}(\omega_1)$$
$$\times[g(E)f(E-\omega_1)-f(E)g(E-\omega_1)]+D^A_{p-p'}(\omega_1)[g^K(E)f(E-\omega_1)-f^K(E)g(E-\omega_1)]\}\delta(-\omega)); \qquad (4)$$

similar expressions can be written for $T^R(E,t)$. In Eq. (4), $\kappa(x)$ is the electron-phonon interaction constant (which depends on coordinate x), index K denotes the Keldysh function,[34] and all functions g and f are diagonal in the energy variable. Equation (4) is in some ways very similar to the electron-phonon collision integral.[34] The only difference between the electron-phonon collison integral[34] and interaction term $P^R_{\text{e-}ph}$ is that the former describes recombination of quasiparticles to the equilibrium state, while the latter describes the influence of inelastic electron-phonon interactions on the dynamics of g and f. Strictly speaking, functions g and f entering Eq. (4) should be obtained as self-consistent solutions of Eqs. (1) and (2). But, for the sake of simplicity, we adopt here the interaction time approximation; then $T^R(E,t) \simeq i\langle g \rangle / 2\tau_E$ and $P^R(E,t) \simeq i\langle f \rangle / 2\tau_E$, where τ_E is the energy-dependent inelastic electron-phonon scattering time[34] determined using the above Eq. (4) in each particular electrode.

We will assume that the thickness of our Al-oxide layers is $d_B \approx 1$ nm. This value is comparable to k_F^{-1} in metals, where k_F is the Fermi wave vector. Since the thickness of the middle N layer satisfies $d_N \simeq \xi_{BCS} \gg k_F^{-1}$, one gets $d_B \ll d_N$. In this case the interface jump of the quasiclassical Green functions is computed from special boundary conditions.[35–37] One can simplify Eqs. (1) and (2) by assuming that the absolute value $|\tilde{\Delta}(x)|$ and phase $\chi(x,t)$ of the SC order parameter $\tilde{\Delta}(x,t)$ vary on different scales. Specifically, since bias voltage $V = (2\pi/\Phi_0)\int^t d\tau \varphi(\tau)$ drops entirely on atomic scale $d_B \sim k_F^{-1}$, the spatial dependence of $\chi(x,t)$ inside each SC layer may be neglected. Here the Josephson phase difference is $\varphi = \chi_1 - \chi_2$; henceforth, indices 1 and 2 refer to left and right S electrodes, respectively. Therefore, with good precision, one may set $\tilde{\Delta}(x,t) \simeq |\tilde{\Delta}(x)| e^{i\chi(t)}$ in Eq. (2). In this approximation time derivatives $\partial/\partial t$ in Eqs. (1) and (2) act only on $\varphi(t)$, while the spatial derivatives result from the variation of "pairing potential" $\tilde{\Delta}(x)$ over a "slow" spatial scale $\sim \xi_{BCS} \gg a$. Sharp jumps of $\tilde{\Delta}(x)$ and the appearance of a finite $V(t)$ at the interfaces are taken into account by applying appropriate boundary conditions.[35] When calculating the discontinuity in the Green functions at the interfaces, one should take into account their dependence on time [in other words, the nondiagonal corrections of kind $\sim g(E, E \pm \Omega)$, where Ω is the frequency of an ac field]. However, in our case, where $\alpha \ll 1$, such nonstationary corrections may be neglected for the following reasons. First, we only consider solutions which are *homogeneous in time*. Such solutions describe a system under the influence of an external dc field, or an ac field of constant amplitude; in most cases, this does not lead to a nonstationary behavior of the system (although the electron distribution function n_E may substantially deviate from equilibrium). Therefore, for $\alpha \ll 1$, if the system is homogeneous in time, its properties, on a sufficiently long time scale $t \gg 1/\Omega$, depend only on $t - t'$, but not on $t + t'$ (where t and t' denote two instants of time). An exception is a nonlinear system which can behave chaotically; however, we do not consider this case here. Thus, for a low-transparency SINIS junction, the nonstationary behavior is related to the time dependence of phase difference $\varphi(t)$ only, while the nonstationary changes in $|\tilde{\Delta}(x)|$ and in the electron excitation spectrum may be neglected.

When a finite-bias voltage $V \neq 0$ is applied across the junction, the ac Josephson effect takes place. The excitation spectrum in the N layer at $V \neq 0$ can then be computed using nonstationary boundary conditions.[35–37] Following Refs. 35–37, the expression for the electric current for a low-transparency interface ($\alpha \ll 1$) is written in the form

$$I = -\frac{p_F^2}{8\pi} \int \frac{dE}{2\pi} \int d^2\rho \, \mathrm{Sp}\hat{\tau}_z \langle \eta \alpha(\eta) \times (\hat{g}_1^R \hat{g}_2^K + \hat{g}_1^K \hat{g}_2^A - \hat{g}_2^R \hat{g}_1^K - \hat{g}_2^K \hat{g}_1^A) \rangle_\eta , \tag{5}$$

where index "$R(A)$" denotes retarded (advanced) matrix Green functions $\hat{g}^{R(A)}$, index "K" denotes the matrix Keldysh Green function $\hat{g}^K$, $\hat{\tau}_z$ is the Pauli matrix, index "1(2)" corresponds to the right (left) S electrode, $\eta = \cos\theta$, where θ is the angle between the electron momentum $\mathbf{p}$ and the $\hat{\mathbf{x}}$-axis, and the brackets in Eq. (5) denote angular averaging. Matrix $\hat{g}^R$ is

$$\hat{g}^R = \begin{pmatrix} g & f \\ -f^* & -g \end{pmatrix},$$

where g and f are the normal and anomalous retarded Green's functions obtained as solutions of Eqs. (1) and (2). In the time domain, the "product" in Eq. (5) is written as

$$(g_1 g_2)_0(t,t) = \int dt' g_1(t,t') g_2(t',t).$$

Index "zero" on the brackets indicates that all the functions should be evaluated in the immediate neighborhood of the boundary, whose transparency is taken in zeroth order in α. The influence of various external fields (including an external magnetic field, bias voltage, ac field etc.) is taken into account by the following gauge transformation:

$$g(t,t') \to e^{i\chi/2} g(t,t') e^{-i\chi'/2}; f(t,t') \to e^{i\chi/2} f(t,t') e^{i\chi'/2},$$

where $\chi(t) = \varphi_0 - (2e/\hbar)\int^t dt V(t)$ and V is the bias voltage applied across the junction.

The above Eq. (5) allows us to compute the electric current across an interface barrier when a finite-bias voltage $V \neq 0$ is applied. In the limit of low transparency, $\alpha \ll 1$, the electric current is expressed in terms of the local electron density of states $\mathcal{N}(E,x) = \mathrm{Re}\, g(E,x)$, the local Cooper pair amplitude $\mathcal{M}(E,x) = \mathrm{Re}\, f(E,x)$, and the electron distribution function n_E. The electron transport across the junction is determined by the interplay between the ordinary reflection and the Andreev reflection. The earlier mentioned processes also modify the electron spectrum in the adjacent electrodes. For single-barrier junctions with semi-infinite electrodes (e.g., SIS or NIS), in most cases, one may use the equilibrium functions, i.e., $\mathcal{N}(E,x) = \mathcal{N}_0(E) = E\theta(E-\Delta)/\sqrt{E^2-\Delta_i^2}$; $\mathcal{M}(E,x) = \mathcal{M}_0(E) = \Delta_i \theta(E-\Delta_i)/\sqrt{E^2-\Delta_i^2}$ (where Δ_i is the proximity-modified magnitude of Δ in the

ith electrode), and $n_E = 1 - 2n_E^F = \tanh(E/2T)$ where n_E^F is the Fermi function. Although such a simplification works well for single-barrier junctions, it is not generally applicable for multibarrier geometries when the proximity interaction range exceeds the distance between different interfaces. The electric current across a multibarrier junction is then determined not only by the local interaction at the nearest interface, but also by the interaction which stems from the more distant interfaces. Such an extension is described in terms of *phase-correlated* Andreev reflection, which makes an *additional contribution* to the total electric current (as compared with conventional current determined by local processes at each separate interface).

In order to simulate the experimental data, we numerically solved Eqs. (1) and (2) for the SINIS geometry and for arbitrary τ_i (but with $\tau_i \gg \hbar/E_F$). We first obtained an equilibrium solution as a trial input for the nonequilibrium case which is considered in the next stage. To find the equilibrium solution, we used the original EE in the Matsubara representation[33] [in Eqs. (1) and (2), this corresponds to setting $\partial/\partial t \equiv 0$, $T^R = 0$, $P^R = 0$, $n_E \equiv \tanh(E/2T)$, and $E + i\delta \to i\omega_n$, where ω_n are the Matsubara frequencies]. After performing the Riccati parametrization,[39] $g_{\omega_n} = (1 - aa^+)/(1 + aa^+)$ and $f_{\omega_n} = 2a/(1 + aa^+)$; the coupled unstable EE are transformed to stable uncoupled Riccati equations[39] that are easily integrated numerically. One then finds the self-consistent solution[40] of Eqs. (1) and (2), and computes the actual equilibrium profile of $\tilde{\Delta}(x)$. In the next stage, equilibrium solution g_{ω_n} and f_{ω_n} is used as a trial input to obtain functions $g(E,x,\eta)$ and $f(E,x,\eta)$ for a fixed dc voltage $V \neq 0$ that allows a determination of the local electron density of states (EDS) $\mathcal{N}(E,x)$, pair amplitude $\mathcal{M}(E,x)$, and electric current I. The solution of Eqs. (1) and (2) is obtained now using the boundary conditions[35–37] (which indeed are applicable for the two-barrier geometry). At this stage functions $T^R(E,t)$ and $P^R(E,t)$ are finite and, for a trial input, are determined using Eq. (4) [and using a similar expression for $T^R(E,t)$] by substituting the equilibrium functions $g^{(0)}(E,x,\eta)$ and $f^{(0)}(E,x,\eta)$ with appropriately shifted energy arguments. The time dependence of the Green functions and of $T^R(E,t)$ and $P^R(E,t)$ for our case, where $\alpha \ll 1$, is determined by phase factors of the kind: $\exp(\pm i\varphi)$, where $\varphi = 2eVt$, and V is the bias voltage. In this way one obtains a numerical solution of Eqs. (1) and (2) for a fixed finite $\varphi \neq 0$. Qualitatively, a variation of the electron incidence angle [described by parameter η in Eqs. (1) and (2)] changes the spatial scale on which the local electron density of states varies. In general, it affects both positions E_n and width Γ_n of the ABS levels. In our problem, we have to average over all possible values of η; the net result of averaging is an increase of the width of the ABS energy level (as compared with the case of $\eta = 1$).

The local EDS was computed for each layer of a SINIS junction. For the sake of simplicity we set $k_B T_c^S = 0.57\Delta_S$ and $T_c^N = 0$ [$T_c^{S(N)}$ is the critical temperature of the bulk S(N) material]. Junction parameters used in the calculations for the ''clean'' N layer (assuming $\Delta\tau_i = 7$) are as follows. The values of the barrier transparency were $\alpha_1 = 2.5 \times 10^{-5}$ and $\alpha_2 \simeq 6 \times 10^{-5}$ (which corresponds to $Z_1 = 0.31$ and $Z_2 = 0.28$, respectively, where $Z_i = V_i/E_F$; V_i is the height of the ith interface barrier). These values correspond to our experimental conditions, determined by comparing with a single $Nb/Al/AlO_x/Al/Nb$ junction fabricated in the same deposition run, and using an empirical dependence of the Josephson critical current on the oxidation dose.[41] The normalized thickness of the N layer, d_N/ξ_{BCS}, is 0.7 (here and below, we express the spatial coordinates in units of ξ_{BCS}). The left and right interface barriers are positioned at $x_{B1} = -0.4$ and $x_{B2} = 0.4$, respectively; the effective width of the quantum potential well formed by the minimum of the superconducting order parameter $\Delta(x)$ in the N electrode is $d_N = 0.9$. Typical results of the calculations for $\eta = 1$ are shown in Fig. 8. Curve 1 is for the local EDS in the left S layer at a distance $x/\xi_{BCS} = 0.1$ from the left barrier, curve 2 shows $\mathcal{N}(E)$ inside the N layer at $x/\xi_{BCS} = 0.1$, curve 3 shows $\mathcal{N}(E)$ in the right S layer at a distance $x/\xi_{BCS} = 0.1$ from the right barrier, and curve 4 corresponds to the EDS of a bulk superconductor, which coincides with the classic BCS density of states. One can see that the local EDS has a sharp maximum at $E/\Delta \simeq 1$ (curves 1–3); this maximum is much narrower and higher compared to the BCS maximum in bulk (curve 4). This maximum is related to the position of an ABS level that is not localized in the N layer alone, but which spreads over the whole SINIS system. The latter is clear from the right-hand inset in Fig. 8, where we show the spatial dependence of the peak height at $E \simeq \Delta$; the peak height jumps at interfaces $x = \pm d_N/(2\xi_{BCS})$, and persists deep into the S electrodes. Such a result agrees well with known analytical results for a SNS junction,[42] from which one may infer that the Green function poles (which correspond to ABS) coincide for adjacent S and N electrodes for $\alpha \simeq 1$. In our SINIS junction, $\alpha \ll 1$; as a result, the poles of the Green function in S and N electrodes do not precisely coincide, but

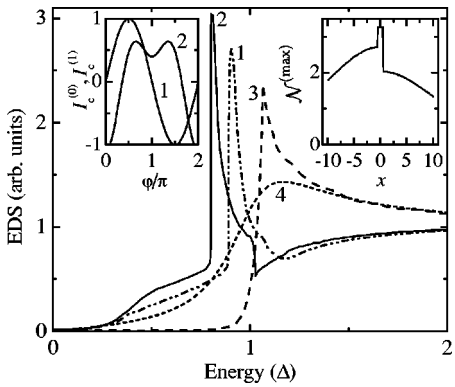

FIG. 8. The local electron density of states (EDS), normalized to the EDS in the normal state, calculated in the left S, N, and right S layers (curves 1–3, respectively); see text for details. Curve 4 corresponds to EDS deep in the bulk S according to the BCS theory. The left-hand inset shows the current-phase relationship for the zero-bias (curve 1) and finite-bias (curve 2) steps. The right-hand inset shows the maximum of the EDS at the ABS level, $\mathcal{N}^{(max)}$, as a function of x (measured from the center of the N layer in the units of ξ_{BCS}).

are still positioned quite close to each other. The results shown in Fig. 8 correspond to case $\varphi=0$ (i.e., when no bias voltage is applied across the SINIS junction). The calculations for finite $\varphi=2eVt\neq 0$ give a quite similar result with one exception. Namely, for $\alpha\ll 1$, we find that the height of a peak positioned at $E/\Delta\simeq 1$ oscillates versus φ, but the peak position remains fixed. The shape of local EDS curves does not change qualitatively when φ varies. For this reason, the ABS singularities are also well pronounced in EDS curves averaged over time. In the experiment, we measure the dc differential tunneling conductivity, which is expressed via time averages of local EDS in adjacent electrodes; therefore, the sharp ABS peaks are clearly observable in the experimental curves [cf. Figs. 3(b), 5, and 6].

The dashed curve in Fig. 3(b) is the differential conductivity obtained as a result of numerical calculations within our theoretical model; the dash-dotted curve is the differential conductivity computed using the BCS electron density of states in *S* electrodes for an equivalent SIS junction. Here the value of the Nb energy gap is taken to be $\Delta_{\mathrm{Nb}}=1.3$ meV. Other parameters used in the calculations are as follows: $\tau_{\mathrm{i}}\Delta=6$ (here τ_{i} is the electron-impurity scattering time); the thickness of the middle N layer is $d_{\mathrm{N}}=0.85$ (measured in units of the BCS coherence length, ξ_{BCS}); $Z_1=0.3$; $Z_2=0.15$ (where $Z_i=V_i/E_{\mathrm{F}}$ with V_i being the height of ith interface barrier and E_{F} being the Fermi energy). One can see that the theoretical curve (dashed curve) well reproduces the main features observed at Δ_{Nb}/e and at $2\Delta_{\mathrm{Nb}}/e$. Note that the BCS electron density of states yields a much wider maximum at $2\Delta_{\mathrm{Nb}}/e$ (see the dash-dotted curve) than that in the experimental curve [solid curve in Fig. 3(b)].

As can be seen from Fig. 8, the ABS level is superimposed on a regular BCS singularity at $E\simeq\Delta$ inside of the Nb electrodes. However, according to our calculations, the ABS produces a much sharper peak in the local EDS as compared to the regular BCS singularity (ideally, it produces a divergence; in reality, the divergence is smeared out by finite temperature and the presence of impurities). Such a difference is clearly seen if one compares curve 4 (showing the EDS inside the bulk Nb without ABS) with curves 1 and 3 in the main part of Fig. 8.

The local EDS computed for a "dirty" SINIS junction ($\Delta\tau_{\mathrm{i}}=0.7$ in the N layer) is shown in Fig. 9 for the N layer and for the right S electrode (curves 1 and 2, respectively). Other parameters used in the calculation are as follows: $d_{\mathrm{N}}=1.2$, $x_{B1}=-0.45$, $x_{B2}=0.45$ (in units of ξ_{BCS}, $Z_1=0.4$, $Z_2=0.2$ (in units of E_{F}). Curve 3 shows the EDS deep in the bulk S electrode, which corresponds to the BCS theory. In curves 1 and 2, in addition to a peak at $E\simeq\Delta$, one can see a peak at $E\simeq 0$, which apparently originates from interference between the Andreev and electron-impurity elastic scattering. Similar zero-energy peaks are observed in the experimental curves shown in Fig. 5 (the main figure and the right inset). As purity parameter $\Delta\tau_{\mathrm{i}}$ decreases, the zero-energy peak becomes more pronounced while the height of a peak positioned at $E\simeq\Delta$ tends to decrease.

The electric current was calculated numerically using Eq. (5). The computed CVC are in good agreement with experimental data (see, e.g., Figs. 1, 2, and 9). The main features of

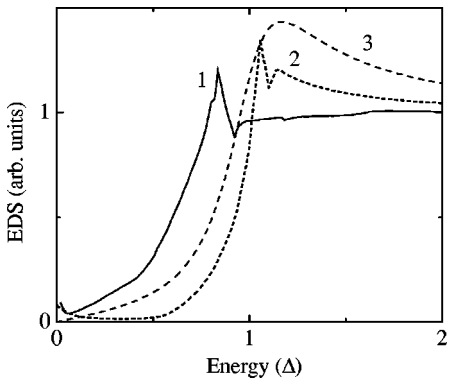

FIG. 9. The local electron density of states (EDS) computed for $\Delta\tau_i=0.7$ (a "dirty" case) in N (curve 1), and in the right S layer (curve 2), respectively. Other parameters are as follows: $d_{\mathrm{N}}=1.2$, $x_{\mathrm{B1}}=-0.45$, $x_{\mathrm{B2}}=0.45$, $Z_1=0.4$, $Z_2=0.2$. Curve 3 corresponds to EDS deeply in the bulk *S* according to the BCS theory.

the CVC also follow from the analytical results. The conventional dc supercurrent at $V=0$ is expressed by Eq. (5), where the retarded (advanced) Green function $\hat{g}_E^{R(A)}$ is obtained as a stationary equilibrium solution of Eqs. (1) and (2). The Keldysh function for $V=0$ is obtained as $\hat{g}_E^K=(\hat{g}_E^R-\hat{g}_E^A)\tanh(E/2T)$. When the bias voltage is finite (i.e., $V\neq 0$) such an equilibrium approximation does not work for two reasons: (i) the retarded (advanced) anomalous Green function $f^{R(A)}(E,\varphi)$ becomes time dependent because φ depends on t and (ii) distribution function n_E at finite-bias voltages deviates from equilibrium. As we shall see below, the above-mentioned nonstationary nonequilibrium effects may lead to qualitatively phenomena not observed earlier, in the double barrier structures. Specifically, they cause a dc Josephson supercurrent at finite-bias voltage $V\simeq\Delta$. The role of nonstationary and nonequilibrium effects in a double-barrier junction can be illustrated using the following description. For the sake of simplicity, let us consider the voltage-bias regime (i.e., the current is a function of a dc bias voltage, V). Then, the time dependence of anomalous retarded (or advanced) function is written simply as $f^{R(A)}(E,\varphi)=f^{R(A)}(E)\exp(i2eVt)$, where a relation $\varphi=2eVt$ is used. In the energy representation, the nonstationary terms give an additional contribution to the dc current:

$$\delta I_s^{(1)}\propto\int dE\int \omega_1 f_1^R(E-eV,E+eV-\omega_1)f_2^{K*}(E-\omega_1,E)$$
$$=\int dE\int \omega_1 f_1^R(E-eV)\,\delta(2eV-\omega_1)f_2^{K*}(E-\omega_1,E), \tag{6}$$

where we used the expression for the nondiagonal in energy, retarded (advanced) anomalous Green function:

$$f^R(E-eV,E+eV-\omega_1)=f^R(E-eV)\,\delta(2eV-\omega_1).$$

The anomalous Keldysh Green function entering Eq. (6) is obtained from the solution of the quantum kinetic equation:[34]

$$\mathbf{v}_F\nabla\hat{g}^K+\hat{\tau}_z\frac{\partial}{\partial t}\hat{g}^K+\frac{\partial}{\partial t'}\hat{g}^K\hat{\tau}_z+\mathcal{L}(t,t')=0, \tag{7}$$

where

$$\mathcal{L}(t,t')=i\int dt_1\{\hat{\Sigma}^R\hat{g}^K+\hat{\Sigma}^K\hat{g}^A-\hat{g}^R\hat{\Sigma}^K-\hat{g}^K\hat{\Sigma}^A\}$$

and $\hat{\Sigma}$ is the self-energy which describes the electron interaction with phonons and impurities.[34] In the last equation, we assumed that, for the low-transparency SINIS junction with $d_N\simeq\xi_{BCS}$, gradient term $\mathbf{v}_F\nabla\hat{g}^K\approx 0$, electromagnetic field vector potential $\mathbf{A}(t)\approx 0$, and $\hat{\Delta}(t)\approx 0$ inside N. At the interfaces, the jump of $\hat{g}^K$ is obtained from the nonstationary boundary conditions.[35–37] Alternatively, the nonstationary influence of adjacent S electrodes on N may be accounted for by a nonstationary source term introduced into Eq. (7). According to Refs.[35,38], for a low-transparency tunneling interface such a term can be written as

$$\hat{I}_T(t,t')=v_T[\hat{g}_1^R\hat{g}_2^K+\hat{g}_1^K\hat{g}_2^A-\hat{g}_2^R\hat{g}_1^K-\hat{g}_2^K\hat{g}_1^A]_{t,t'},$$

where v_T is the tunneling frequency. From Eq. (7), one obtains an expression for the anomalous Keldysh function:

$$(2E-\omega)f^K(E,E-\omega)=2\Delta g(E,E-\omega)+\hat{I}_T^{12}(E,E-\omega)+\mathcal{L}^{12}(E,E-\omega),$$

where $\hat{I}_T^{12}$ and $\mathcal{L}^{12}$ stand for the nondiagonal matrix elements of $\hat{I}_T$ and $\mathcal{L}$. From the last equation, $f^K_{E,E-\omega}$ in N is evaluated as

$$\begin{aligned}f^K_{E,E-\omega}&\simeq\frac{\hat{I}_T^{12}(E,E-\omega)}{2E-\omega+i/\tau_E}\\&=v_T\frac{2}{2E-\omega+i/\tau_E}\\&\quad\times[g_1(E)f_2(E-\omega)\delta n_E+f_1(E)\\&\quad\times g_2(E-\omega)\delta n_{E-\omega}],\end{aligned} \tag{8}$$

where $g_1(E)$ and $f_2(E)$ denote the diagonal in E retarded normal and anomalous Green functions taken from the left and right sides of the barrier. Equation (7) also gives the kinetic equation for the nonequilibrium distribution function n_E in the form:

$$I_T^{(i)}(E)+\mathcal{L}_{ph}^{(i)}(E)=0, \tag{9}$$

where the tunneling source in the ith electrode is:[38]

$$I_T^{(i)}(E)=v_T[g_i(E)(n_{-E-V}-n_{E-V}+2n_E)+(n_{-E-V}-n_{E-V})\theta(E^2-\Delta^2)].$$

For the electron-phonon collision integral $\mathcal{L}_{ph}(E)$ in the ith electrode, one uses an approximate expression:

$$\mathcal{L}_{ph}^{(i)}(E)=\frac{g_i(E)}{\tau_E}\left(n_E-\tanh\frac{E}{2T}\right). \tag{10}$$

The recombination time of quasiparticles, τ_E, is strongly dependent on the energy. In particular, it rises sharply at $E\simeq E_n$, and is much smaller at other energies, $E\neq E_n$. Therefore, the solution of Eq. (9) corresponds to a nonequilibrium distribution function n_E having a sharp peak at the ABS position, $E\simeq E_n$. Then, at $V\simeq E_n$, the deviation of n_E from equilibrium, $n_E^{(0)}=\tanh(E/2T)$, is found to be

$$\delta n_E=n_E-\tanh\left(\frac{E}{2T}\right)\simeq\kappa v_T\tau_E\delta(E-E_n), \tag{11}$$

where the dimensionless factor κ depends on the particular SINIS geometry and electrode purity. Substituting Eq. (11) into the nondiagonal anomalous function (8) and using it in term (6), one obtains a nonstationary contribution to the dc supercurrent of the kind:

$$\begin{aligned}\delta I_s^{(1)}&\propto\int dE\int\omega_1 f_1^R(E-eV)\delta(2eV-\omega_1)f_2^{K*}(E-\omega_1,E)\\&\simeq\kappa v_T^2 f_1(E_n-2eV)g_2(E_n)\left[\frac{\tau_{E_n}|E_n-eV|}{(E_n-eV)^2+1/4\tau_{E_n}^2}f_1(E_n-eV)+\frac{\tau_{E_n-eV}|E_n-2eV|}{(E_n-2eV)^2+1/\tau_{E_n-eV}^2}f_2^*(E_n-eV)\right],\end{aligned} \tag{12}$$

where we assumed $v_T\tau_{E_n}\gg 1$; we also neglected small nonresonant terms. When evaluating $\delta I_s^{(1)}$, one should take into account the energy dependence of the recombination time, τ_E, which is quite large at the narrow ABS level E_n. The sharp energy dependence of τ_E produces the singularity in Eq. (12) at $eV=E_n$ (the width of which is $\sim 1/\tau_{E_n}$). There is also a similar singularity at $eV=E_n/2$, but it is much less pronounced as compared to the former one, because $\tau_{E_n-eV}\ll\tau_{E_n}$ at $V=E_n/e$; it might be observed in the CVC of high-transparency double-barrier junctions (not considered here).

The above expression (12) describes a system where n ABS levels are present. As follows from our calculations, in the case of a realistic SINIS junction only one ABS level, E_A, is present at $E\simeq\Delta$. The singularity in Eq. (12) at

$eV=E_A$ is responsible for the appearance of a new source of phase-coherent supercurrent in a SINIS junction, which is observed in the CVC as a current step at $V=\Delta/e$; we call this phenomenon the Finite-Bias Josephson Effect (FBJE). As follows from the derivation given above, the FBJE originates from a nonequilibrium population of the ABS level by Cooper pairs when an external dc bias voltage is applied.

More accurate calculations of the supercurrent were carried out numerically. The total electric current indeed shows a two-step structure: the first step being an ordinary dc Josephson current at $V=0$ [associated with the ''energy band'' $E_J(1-\cos\varphi)$, where E_J is the Josephson coupling energy], and the second step being due to the FBJE [associated with the *second* band $E'_A(\varphi)=\int_0^\varphi d\varphi' I_s^{(1)}(\varphi')$, consistent with the experimental observation (cf. Fig. 1)].

Although the effect becomes stronger if the temperature is decreased below the temperature of the intrinsic superconducting transition of the N layer, the anomalous current ($\propto f_1 f_2^\dagger$) persists even if *pairing potential* $\Delta(x)$ vanishes in N, because $f(x)$ (related to the *pair amplitude*) remains finite due to the proximity effect.

Our self-consistent solution [taking into account ''smearing out'' of $\Delta(x)$ at the interfaces] shows that the position of the ABS level is rather insensitive to changes of the Al interlayer thickness; i.e., even if the thickness d_N significantly deviates from ξ_S, the position of the ABS level will not strongly deviate from Δ/e. This result is in agreement with the experiment. On the contrary, a non-self-consistent approach [using, e.g., solution of the Bogolyubov equations and a sharp $\Delta(x)$ profile] results in a high sensitivity of the energy-level structure to the thickness of the Al interlayer. Qualitatively, the favored position of the ABS level at $E_A \simeq \Delta$ arises from the well-known fact that for small σ, the probability of the AR is maximum at $E\simeq\Delta$,[43] and is small at other energies.

Magnitudes $I_c^{(0)}$ and $I_c^{(1)}$ for the steps in the critical supercurrent (observed in the experimental CVC at $V=0$ and $V\simeq\Delta/e$, respectively) depend on H in an oscillatory way, since they are proportional to the nonequilibrium population of CP on the ABS level at $E\simeq E_A$. The experimental $I_c^{(1)}(H)$ dependence is understood if one considers anharmonic terms in the expression for $I^{(1)}(\varphi)$: $I^{(1)}(\varphi)=I_c^{(1a)}\sin(\varphi+\varphi_1)+I_c^{(1b)}\sin(2\varphi+\varphi_2)+I_c^{(1c)}\sin(\varphi/2+\varphi_3)$, where $I_c^{(1a)}$ and $I_c^{(1b)}$ are determined numerically at $V\simeq\Delta/e$ [see the left inset in Fig. 8 where we compare the computed $I_c^{(0)}(\varphi)$ (curve 1) and $I_c^{(1)}(\varphi)$ (curve 2)]; term $I_c^{(1c)}$ was introduced to better fit the height of the maxima in the experimental $I_c^{(1)}(H)$ dependence. Although this term does not follow from our current theory, it may appear in the real system as a result of a parametric nonlinear interaction of the Josephson junction with its own ac field. For our experimental conditions we find $I_c^{(1a)}=1.7$, $I_c^{(1b)}=1.15$, $I_c^{(1c)}=0.6$, $\varphi_1=\pi/2$, $\varphi_2=-\pi/2$, $\varphi_3=-\pi/2$. The theoretical $I_c^{(1)}(H)$ dependences with and without the $I_c^{(1c)}$ term are shown in Fig. 2(b) as curves 1 and 2, respectively, along with the conventional $I_c^{(0)}(H)$ dependence (curve 3). Reasonable agreement between theoretical curve 2 with the experimental $I_c^{(1)}(H)$ data [solid circles in Fig. 2(a)] is seen. The complicated shape of the $I_c^{(1)}(H)$ dependence is caused by a significant contribution of the $I_c^{(1b)}\sin(2\varphi+\varphi_2)$ term.

To examine how the onset of superconductivity in the middle N layer influences the FBJE, we compared the experimental temperature dependence of the step height (see scatter plot in Fig. 4) with the theoretical temperature dependence of the partial critical current $\mathcal{I}_c^{(1)}(T)$ (solid curve in Fig. 4). The theoretical dependence is calculated from Eqs. (5), where the Josephson part is $\propto f_1 f_1^\dagger$. In the experimental dependence, one sees a steep rise of the step height as the temperature decreases in the range between 1.85 K and 1.95 K, which may be associated with the superconducting transition of the N layer.[11,30] The theoretical dependence was calculated using an Al critical temperature $T_c^{Al}=1.9$ K. The theory qualitatively reproduces the behavior observed in the experiment, in particular, a considerable decrease of the step height when the middle Al electrode becomes normal. For $T>T_c^{Al}$, the step is substantially depressed, but it does not vanish completely [as can be seen from Fig. 3(b)]. Such a behavior indicates that transport through ABS levels may exist in the double-barrier devices even for $T>T_c^{Al}$. Although the ABS band structure is changed when the middle electrode becomes superconducting, the underlying basic physical processes responsible for electrical transport are very similar in both cases.

IV. DISCUSSION

We now discuss in more detail the physical origin of the ABS structure and its relation to the experimentally measured conductivity of SINIS junctions. Physically, the ABS structure is caused by quasiparticle interference involving both ordinary and Andreev reflections in the potential well (with width $d_N\simeq\xi_{BCS}$) formed by the $\Delta(x)$ profile. For $E\simeq\Delta$, the walls of the potential well become smeared out, which, for $d_N\leqslant\xi_{BCS}$, tends to keep the ABS level position at $E\simeq\Delta$. According to Figs. 8 and 9 a sharp singularity at $E\simeq\Delta$ is present in the local EDS of adjacent N and S electrodes. Also from Figs. 8 and 9 one may infer that the ABS peak positions are slightly different in N and S (inside N the ABS level position is slightly lower than it is in *S*). Curve 1 in Fig. 10(b) shows the experimental differential conductivity of a SINIS junction whose CVC is given in Fig. 10(a). The experimental data were numerically fitted [curve 2 in Fig. 10(b)] using our theoretical model with the following parameters: $d_N=0.95$, $x_{B1}=-0.35$, $x_{B2}=0.35$, $Z_1=0.35$, $Z_2=0.15$ and $\Delta\tau_i=5.7$. The lower peak at $V\simeq1.7\Delta_{Nb}/e$ [see curve 2 in Fig. 10(b)] corresponds to a resonance at $V_d=(E^S_{A(1)}+E^N_A)/e$ (here $E^S_{A(1)}$ and E^N_A are the ABS level positions inside the left S and the N electrodes, respectively) in the quasiparticle tunneling between the ABS singularities in adjacent electrodes. The upper peak in curve 2 is related to a similar resonance at $V_d=(E^S_{A(1)}+E^S_{A(2)})/e$ (where $E^S_{A(2)}$ is the ABS level position in the right electrode). Curve 3 in the Fig. 10(b) corresponds to the differential conductivity of an equivalent SIS junction (i.e., having the same superconducting parameters for the S electrodes as the SINIS junction

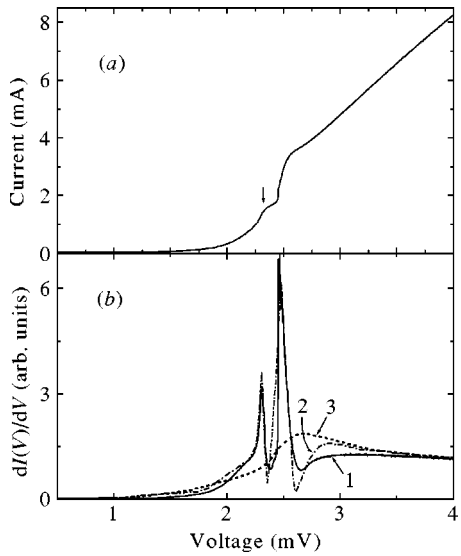

FIG. 10. (a) Typical CVC of a Nb/Al/AlO_x/Al/AlO_x/Nb junction at $T=1.8$ K which displays a ''gap-difference'' feature (marked by the arrow). (b) Experimental differential conductivity of the same junction (curve 1) in comparison with theoretical curve 2 obtained for a SINIS junction with $d_N=0.95$, $x_{B1}=-0.35$, $x_{B2}=0.35$, $Z_1=0.35$, $Z_2=0.15$, and $\Delta\tau_i=5.7$. Curve 3 is the differential conductivity computed using the BCS density of states in *S* electrodes.

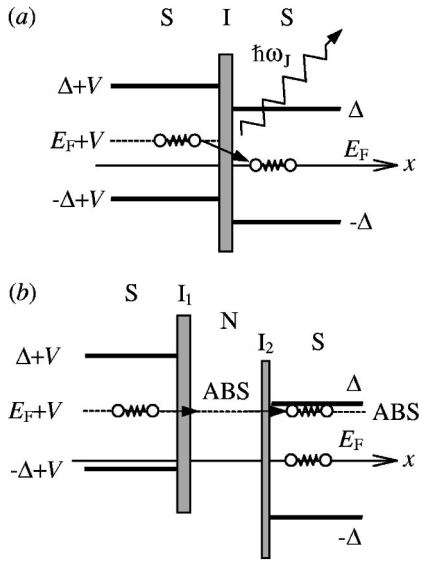

FIG. 11. Schematic diagram showing: (a) nonstationary Josephson effect at $V\neq 0$ in a SIS junction and (b) tunneling processes that contributes to the phase-coherent dc current at $V\simeq E_A$ in an SINIS junction.

has), as obtained using the BCS density of states; one can see that the BCS peak at $V\simeq 2\Delta_{Nb}/e$ is much broader than the ABS-related peaks.

We suggest that the calculated splitting in the ABS level positions $\propto E_A^S-E_A^N$ has been observed in the experimental differential conductivity curves at sufficiently low temperatures [see dI/dV curves at 1.8 and 2.5 K in Fig. 5, and experimental curve 1 in Fig. 10(b)]. Indeed, theoretical curve 2 in Fig. 10(b) qualitatively reproduces all the main features observed in experimental curve 1 quite well. Here, the experimental curve is shown for 1.8 K, whereas the theoretical curve is calculated for 2.2 K. In the calculations, the temperature was regarded as a fitting parameter to account for a possible self-heating of the sample during the experiment by the bias current at a voltage close to the gap-sum voltage. Using $T=1.8$ K in the calculations gives a slightly larger splitting of the two peaks.

Note that the additional feature that often appears in the CVC of SINIS junctions above the T_c of Al [as marked by an arrow in Fig. 10(a)], at a voltage, slightly lower than the gap-sum voltage was earlier explained as a gap-difference feature resulting from an extreme superconducting gap enhancement in the Al due to nonequilibrium tunnel extraction of quasiparticles.[24] On the basis of empirical observations on similar junctions, one of the authors of this paper suggested that the feature may be due to a peak in the density of states of Al, but without an accompanying energy gap.[32] It appears now that the theory presented here indeed yields the structure observed in the experiment, and that the underlying physical mechanism does not require a superconducting energy gap in the Al. Therefore, the present theory offers an alternative to the ''classical'' explanation of the origin of the feature given by Blamire *et al.*[24] Since this is an important physical issue (pertinent to the question of whether or not an attractive pairing potential does exist in a superconductor far above T_c), additional, more direct, experiments are needed to clarify the origin of the feature.

The presence of sharp ABS levels in the excitation spectrum of SINIS junctions affects not only the quasiparticle component of electric current, but the Josephson component of current as well. Specifically, the ABS level at $E\simeq\Delta$ results in the second Josephson current step at $V\simeq\Delta_{Nb}/e$ (see Fig. 1), which is unique to SINIS junctions. For ordinary lumped SIS junctions, there is only the one current step at $V=0$; for $V\neq 0$, the dc Josephson current turns into an oscillating current with frequency $\omega_J=2eV/\hbar$. As a result, each Cooper pair (CP) loses energy $E_1-E_2=2eV$ on traversing the junction, and recombines into the superfluid condensate. The energy lost, $\hbar\omega_J$, is radiated into the environment [see Fig. 11(a)] as an electromagnetic wave. The recombination process occurs in a time of order $\tau_{rec}\simeq\hbar/\Delta$, and on a short distance of order $\sim\xi_{BCS}$ (where $\xi_{BCS}=\hbar v_F/\pi\Delta$ is the BCS coherence length). However, a different scenario may take place in SINIS junctions where an ABS level may appear at a finite energy $E=E_A\neq 0$. Width Γ_n of the ABS peak at $E/\Delta\simeq 1$ is related with rate τ_{ABS}^{-1} of quasiparticle recombination from the upper localized ABS level into the superfluid condensate and is very small, $\Gamma_n=\hbar(\tau_{ABS}^{-1}+\tau_{esc}^{-1})\simeq 0.1\Delta$. Consequently, the lifetime of quasiparticles in this ABS level is quite long, about $10\hbar/\Delta$. The corresponding recombination length $l_{ABS}\simeq 10\xi_{BCS}$ is also quite large. Therefore, each of the two phase-correlated electrons injected from the left electrode reside in the ABS level for a relatively long time [see Fig. 11(b)], which may considerably exceed their escape time $\tau_{esc}=(d_N+d_S)/v_F$ (where d_S is the thickness of each of the S layers) from the junction region to the external circuit; i.e., a fraction of Cooper pairs

leave the junction region before recombination occurs while still carrying a finite energy $\simeq 2eV$ per each pair. The energy of the injected pairs in the junction region is preserved, resulting in a *dc nonequilibrium supercurrent* carried by injected pairs at a *finite-bias voltage* $V \simeq E_A/e$ (FBJE), along with the ordinary ac supercurrent $\propto I_c^{(0)} \sin \omega_J t$. Such a situation may take place in an SINIS junction under condition $\tau_{rec} > \tau_{esc}$ (an even more favorable condition, $\tau_{rec} \gg \tau_{esc}$, can be achieved by appropriately adjusting the junction geometry).

The ABS peaks in the electron density of states become suppressed when the concentration of nonmagnetic impurities increases. The reason for this behavior is that electron momentum **p** becomes a ''bad'' quantum number in the ''dirty'' case, in contrast to the ''clean'' case, where **p** may be regarded as a ''good'' quantum number. If the electron-impurity collisions become frequent (i.e., $\Delta \tau_i \ll 1$), **p** is not conserved, and the conditions for forming sharp ABS energy levels become unfavorable.

A qualitative picture of the nonequilibrium supercurrent associated with the subgap step (cf. Fig. 1) can be understood if one takes into account some peculiar features of the SINIS structure, which we mentioned in Sec. III: (i) the probability of Andreev reflection at the NS interface has a peak at $V = \Delta/e$ and, at this point, may be comparable with that of the pure NS interface and (ii) due to the presence of the second barrier, a coherent transport process is possible at this voltage, if the Fermi level of one S layer is aligned with the ABS level of the counterpart NIS structure at $V \simeq \Delta/e$ (which can be achieved using ''asymmetric'' SINIS structures, where the two barriers have slightly different transparencies). This, according to our theoretical model, will lead to stabilization of the phase difference between the S electrodes and, as a consequence, to stabilization of the ABS level position (the phases between the S electrodes normally become uncorrelated when the current through the junction exceeds the ordinary Josephson critical value $I_c^{(0)}$; the energy of the ABS levels, if present, will then oscillate with time[44]). As a result, a stationary Josephson current may flow at this particular voltage. Similar stabilization of the phase difference may occur in an ordinary SIS junction, for example, as a result of a spatial resonance, leading to the well-known Fiske steps in the CVC;[45] the steady-state solution of the equation for the phase is then applicable.[46] In the latter case, however, no additional source of the Josephson current appears at the step.

As can be noticed from the theoretical plot [dashed curve in Fig. 3(b)], the first sharp feature in the conductivity is positioned slightly above the Δ_{Nb} value, because the peak in the nonequilibrium distribution function of phase-correlated electrons injected into an ABS level from the adjacent S electrode happens at energy slightly higher than Δ_{Nb}. The second feature, which originates from a quasiparticle tunneling between two sharp ABS singularities (one of them localized in the N electrode, while the other in the adjacent S electrode) is situated slightly below the $2\Delta_{Nb}$ value, because the ABS level energy in Al is lower than Δ_{Nb} [in agreement with experimental data shown by solid curve in Fig. 3(b)].

The negative slope of the CVC at the onset of the step (see Fig. 1) is not described by the above theory, because the theory implies the voltage-biased regime (which is easier to treat theoretically), whereas the current-biased regime (which is easier to realize in practice) was used in the experiment. The negative slope may be related with the conversion of a fraction of the dissipative current to a nondissipative current when the bias energy reaches the upper ABS level. In an ideal case, all the current becomes nondissipative, and the junction can eventually ''switch'' back to a zero-voltage state. In practice, the system may oscillate between the two states (corresponding to $V=0$ and $V \simeq \Delta/e$). This oscillatory behavior was likely observed by one of the authors in an earlier experiment.[32]

From Fig. 1, one can see that the step at Δ_{Nb} may have multiple branches. This fine structure is also not described by the theory presented here. We suggest that the observed behavior may also be attributed to the complex electrodynamic of the system in the current-bias regime.

We now discuss alternative physical mechanisms for the experimentally observed steplike feature at $V \simeq \Delta_{Nb}/e$.

(i) Suppose that intrinsic superconductivity of the middle Al is present, so that the two supercurrent steps, one at $V=0$ and the second at $V \simeq \Delta_{Nb}/e$, appear as a result of sequential switching to the resistive state of the two Josephson junctions. However, as we discussed in the preceding section, this possibility should be ruled out; although a transition to the superconducting state of the N layer enhances the effect, a trace of the step persists up to temperatures considerably higher than any reasonable T_c for the N layer.

(ii) One could ask if the step is caused by a Fiske resonance; however, the voltage position of the step does not depend on the junction size. Moreover, although the dc component of the ac Josephson current may be high at $V \simeq \Delta_{Nb}/e$ due to increased dissipation of the ac field at this voltage, it cannot exceed the I_c value for lumped junctions.[46] We estimate that the Josephson penetration depth λ_J for our most transparent junctions with $j_c \simeq 1$ kA/cm^2 (considered here) is $\geqslant 10\mu$ (assuming that the London penetration depth $\lambda_L \simeq 100$ nm for Nb films). This means that the current is nearly homogeneously distributed over the area of the junction, so that the dc component of the ac Josephson current cannot exceed the I_c value. However, as can be seen from Figs. 1(a) and 2(a), the height of the second step may exceed the I_c value considerably (the difference is especially pronounced in the case described in Ref. 11). Therefore, a step of this height may only occur if an additional source of the Josephson current turns on at a voltage $V \simeq \Delta_{Nb}/e$.

(iii) Another phenomenon that should be discussed is the well-known multiple Andreev reflection (MAR).[47–51] Such a phenomenon was observed in numerous experiments involving various types of superconducting weak links. In the experimental CVC, it is observed as a series of steplike features at bias voltages $V = 2\Delta/ne$, where n is an integer.[48,49] A necessary condition for the structure to appear is the presence of atomic-size direct-conductivity channels, or a very high (close to unity) transparency of the interfaces (in case of SNS junctions).[48,50,51] We have already pointed out above that the MAR-associated structure has a very low amplitude for our experimental system due to the low transparency $\alpha_{1,2}$

$\sim 10^{-5}$ of the SN interfaces (unlike the systems cited above). Note that, not only the step at $V=\Delta_{Nb}/e$ (cf. Fig. 1), but also the gap structure at $V=2\Delta_{Nb}/e$ [cf. Figs. 1(b), 5, and 10(b)] differ in shape from the MAR features reported earlier. Specifically, the peak at $V=2\Delta_{Nb}/e$ in the conductivity is very narrow and sharp, unlike the ordinary MAR features.[47,48] The experimentally observed features in the conductivity of our SINIS junctions are also different from those recently described theoretically by Brinkman and Golubov.[16] These authors considered coherent effects in SINIS junctions, but they concentrated on the ordinary Josephson current at zero voltage, along with the single-electron excitation current. As a result, they obtained a MAR structure which must be very weak for low-transparency barriers at the interfaces.

Although we considered the simplest case where only one pronounced ABS energy level appears at $E_A \simeq \Delta$ in a double barrier SINIS junction, the real situation may be more complicated. Additional levels at finite energy may appear (and contribute to the features in the CVC) if the thickness of the middle N electrode becomes significantly larger than the coherence length. This case, however, is harder to realize in the experiment for technical reasons.

V. CONCLUSIONS

Experimental data obtained on the SINIS junctions (based on Nb and Al) strongly indicate the presence of substantial contribution from coherent processes to the transport characteristics. This contribution is seen both in the ''superconducting'' branch of the current-voltage characteristic (most striking evidence is a current step at a finite dc voltage $V=\Delta/e$), as well as in the ''quasiparticle'' branch (a narrow, as compared with the width of the BCS singularity, peak at $V=2\Delta/e$, which may split into two peaks at lower temperatures). The proposed theoretical model provides a qualitative explanation of these and other experimental facts (such as a zero-bias anomaly observed on some samples) using the idea that interference effects involving coherent Andreev reflections play an important role in the transport properties. In particular, a novel current step at a finite dc voltage $V=\Delta/e$ is interpreted as a phase-coherent dc supercurrent injected into a narrow ABS energy level. A specific shape of the Fraunhofer pattern for this effect, which we call the Finite-Bias Josephson Effect (FBJE), is explained by an unconventional current-phase relationship for the anomalous supercurrent component responsible for the observed current step. The theory also qualitatively describes the temperature dependence of the supercurrent related with the FBJE, taking into account the onset of intrinsic superconductivity in the middle N layer.

The narrow peak in the differential conductivity at $V=2\Delta/e$ is explained as a consequence of a sudden increase of the quasiparticle current associated with injection into a resonant ABS level situated near energy Δ. The energy position of the level is slightly different for the N and S layers; as a result, the differential conductivity of a SINIS junction may have two features near voltage $V=2\Delta/e$. Such a property suggests an alternative explanation of a feature interpreted earlier as gap-difference feature associated with a superconducting energy gap in the middle Al layer arising from tunneling-extraction of quasiparticles from this layer.

Our results also suggest that the distinction between the superconducting and quasiparticle branches of the current-voltage characteristic, as it was made for the ordinary SIS tunnel junctions, is rather conditional in case of the SINIS junctions.

ACKNOWLEDGMENTS

The authors would like to thank A. A. Golubov and A. Shelankov for useful discussions. This work was supported by the Office of Naval Research under Grant No. N00014-00-1-0025 and by the National Science Foundation under Grant No. EIA-0218652.

*Also with Institute for Metal Physics NASU, 03680 Kyïv, Ukraine.
†Also with Institute of Magnetism NASU, 03142 Kyïv, Ukraine.
‡Also with Department of Electrical and Computer Engineering and Materials Research Center, Northwestern University, Evanston, Illinois 60208.

[1] J. Low Temp. Phys. **118**, Nos. 5/6 (2000), special issue: *Proceedings of the International Conference on Electron Transport in Mesoscopic Systems*, ETMS' 99, August 12–15, 1999, Göteborg, Sweden.
[2] T.M. Klapwijk, Physica B **197**, 481 (1994).
[3] P.F. Bagvell, R. Riedel, and L. Chang, Physica B **203**, 475 (1994).
[4] A.F. Andreev, Sov. Phys. JETP **19**, 1228 (1964).
[5] I.O. Kulik, Sov. Phys. JETP **30**, 944 (1970).
[6] A.F. Morpurgo, B.J. van Wees, T.M. Klapwijk, and G. Borghs, Phys. Rev. Lett. **79**, 4010 (1997).
[7] V.C.Y. Chang and C.S. Chu, Phys. Rev. B **55**, 6004 (1997).
[8] H.T. Ilhan, H.V. Demir, and P.F. Bagwell, Phys. Rev. B **58**, 15 120 (1998).
[9] I.P. Nevirkovets and S.E. Shafranjuk, Phys. Rev. B **59**, 1311 (1999).
[10] I.P. Nevirkovets, J.B. Ketterson, and S. Lomatch, Appl. Phys. Lett. **74**, 1624 (1999).
[11] I.P. Nevirkovets, J.B. Ketterson, S.E. Shafranjuk, and S. Lomatch, Phys. Lett. A **269**, 23 (2000).
[12] I.P. Nevirkovets, J.B. Ketterson, and M. Siegel, IEEE Trans. Appl. Supercond. **11**, 1138 (2001).
[13] S.E. Shafranjuk, I.P. Nevirkovets, and J.B. Ketterson, Solid State Commun. **121**, 457 (2002).
[14] G. Carapella, G. Costabile, and R. Latempa, J. Phys.: Condens. Matter **12**, L1 (2000).
[15] K.-T. Kim, J. Kim, S.-I. Park, and V.D. Koutovoi, J. Korean Phys. Soc. **36**, 453 (2000).
[16] A. Brinkman and A.A. Golubov, Phys. Rev. B **61**, 11 297 (2000).
[17] G.A. Gogadze and A.M. Kosevich, Low Temp. Phys. **24**, 540 (1998).
[18] E. Bartolomé, A. Brinkman, J. Flokstra, A.A. Golubov, and H. Rogalla, Physica C **340**, 93 (2000).
[19] H. Courtois, Ph. Gandit, D. Mailly, and B. Pannetier, Phys. Rev. Lett. **76**, 130 (1996).
[20] A. Frydman and R.C. Dynes, Phys. Rev. B **59**, 8432 (1999).

[21] T. Hoss, C. Strunk, T. Nussbaumer, R. Huber, U. Stauer, and C. Schönenberger, Phys. Rev. B **62**, 4079 (2000).
[22] T.I. Baturina, Z.D. Kvon, and A.E. Plotnikov, Phys. Rev. B **63**, 180503 (2001).
[23] W.M. van Huffelen, T.M. Klapwijk, D.R. Heslinga, M.J. de Boer, and N. van der Post, Phys. Rev. B **47**, 5170 (1993).
[24] M.G. Blamire, E.C.G. Kirk, J.E. Evetts, and T.M. Klapwijk, Phys. Rev. Lett. **66**, 220 (1991).
[25] I.P. Nevirkovets, J.E. Evetts, and M.G. Blamire, Phys. Lett. A **187**, 119 (1994).
[26] E. Goldobin and A.V. Ustinov, Phys. Rev. B **59**, 11 532 (1999).
[27] R. Monaco, A. Polcari, and L. Capogna, J. Appl. Phys. **78**, 3278 (1995).
[28] Experimental data on the $I_c^{(1)}(H)$ dependence were reported by the authors in Ref. 13, but the detailed physical interpretation of the data was not presented.
[29] L. Capogna and M.G. Blamire, Phys. Rev. B **53**, 5683 (1996).
[30] I.P. Nevirkovets and J.B. Ketterson, Inst. Phys. Conf. Ser. **167**, 181 (2000).
[31] Sometimes such a gap-difference-like feature appears even at 4.2 K, as observed by Blamire *et al.*,; see Ref. 24.
[32] I.P. Nevirkovets, Phys. Rev. B **56**, 832 (1997).
[33] G. Eilenberger, Z. Phys. **214**, 195 (1968).
[34] A.I. Larkin, Yu.N. Ovchinnikov, Zh. Eksp. Teor. Fiz. **73**, 299 (1977).
[35] A.V. Zaitsev, Sov. Phys. JETP **59**, 1015 (1985).
[36] M. Eschrig, Phys. Rev. B **61**, 9061 (2000).
[37] A. Shelankov and M. Ozana, Phys. Rev. B **61**, 7077 (2000).
[38] I.E. Bulyzhenkov and B.I. Ivlev, Sov. Phys. JETP **47**, 115 (1978).
[39] N. Schopohl and K. Maki, Phys. Rev. B **52**, 490 (1995).
[40] W. Belzig *et al.*, Superlattices Microstruct. **25**, 1251 (1999).
[41] H. Sugiyama *et al.*, Jpn. J. Appl. Phys., Part 2 **36**, L1157 (1997).
[42] A. V. Svidzinsky, *Space-inhomogeneous Issues of the Superconducting Theory* (Science, Moscow, 1982).
[43] G.E. Blonder, M. Tinkham, and T.M. Klapwijk, Phys. Rev. B **25**, 4515 (1982).
[44] Our calculations show that the amplitude of the oscillations of $E_A(t)$ is small as compared with Δ in the case of low-transparency barriers.
[45] K. K. Likharev, *Dynamics of Josephson Junctions and Circuits* (Gordon & Breach, New York, 1986).
[46] I.O. Kulik, Sov. Phys. Tech. Phys. **12**, 111 (1967).
[47] K. Flensberg, J. Bindslev Hansen, and M. Octavio, Phys. Rev. B **38**, 8707 (1988).
[48] A.W. Kleinsasser, R.E. Miller, W.H. Mallison, and G.B. Arnold, Phys. Rev. Lett. **72**, 1738 (1994).
[49] N. van der Post, E.T. Peters, I.K. Yanson, and J.M. van Ruitenbeek, Phys. Rev. Lett. **73**, 2611 (1994).
[50] E.N. Bratus, V.S. Shumeiko, and G. Wendin, Phys. Rev. Lett. **74**, 2110 (1995).
[51] D. Averin and A. Bardas, Phys. Rev. Lett. **75**, 1831 (1995).